Power Electronics and Drives
Volume 11(46), 2026 DOI: 10.2478/pead-2026-0002

Power Electronics and Drives

Analysis of Open-Loop Current Estimators for Current Sensor Fault Compensation in PMSM Motor Drive

Research paper

Krystian Teler*

Department of Electrical Machines, Drives and Measurements, Wroclaw University of Science and Technology, Wrocław, Poland

Received: 03 December, 2025; Received in the revised form: 16 December, 2025; Accepted: 17 December, 2025

Abstract: The growing demand for fault-tolerant systems requires the use of algorithms that will maintain continuity of operation in the event of faults, e.g., in measuring sensors. Sensorless control methods, originally developed for electric motor drives without speed measurements, can be applied within fault-tolerant control (FTC) strategies when speed sensors fail. Recent research also increasingly addresses failures of current sensors (CS). This study proposes a permanent magnet synchronous motor (PMSM) drive control method based on a current-sensorless vector control structure, eliminating the need to measure phase currents and enabling compensation for damaged CS. Three open-loop estimator types derived from a PMSM mathematical model are introduced, all operating without feedback from state variables. The first estimator uses fixed design parameters optimized via particle swarm optimisation (PSO). The second relies on the relationship between stator flux and dq-axis currents. The third extends this relationship by incorporating rotor position to account for spatial harmonics. The relevant flux functions are stored in look-up tables (LUTs). This study discusses challenges in selecting estimator parameters and issues related to voltage and speed measurement. The proposed solutions were tested on a 2.5 kW PMSM experimental setup across a wide range of operating conditions.

Keywords: *PMSM motor • current sensor faults • stator currents estimation • flux maps • sensorless control*

1. Introduction

The use of converter drive systems in technological processes requires the implementation of vector control structures, such as field-oriented control (FOC) and direct torque control (DTC). Regardless of the motor type (typically induction motor (IM) or PMSM), information about the values of stator phase currents and rotational speed or angular position in the case of speed control is used to determine control signals. The elimination of sensors aimed at analytical redundancy has resulted in the development of a number of sensorless control methods over the years that involve the use of speed estimation techniques. This was mainly justified by economic considerations, such as the high cost of sensors, as well as the need to consider additional mounting space (Holtz, 2006).

Currently, methods are also being sought to reproduce phase currents, whose information is essential for the proper operation of a vector-controlled drive. The need to have information about the current value is further dictated by safety considerations. However, during the operation of the drive under varying operating conditions, these sensors are subject to defects that interfere with the output information or cause it to lose altogether. The impact of faulty current sensors (CS) on drive operation was analysed in Teler et al. (2025a). The consequence of using information from a defective sensor in feedback can be a change in the drive's operating point and even loss of stability (failure).

Current sensor fault-tolerant control (CSFTC) is a therefore critical strategy for maintaining electric motor drive performance during sensor failures, enabling continuous operation through advanced fault detection and system

* Email: krystian.teler@pwr.edu.pl

reconfiguration techniques. Researchers have developed sophisticated methods to detect and mitigate CS faults across various motor types. Key approaches include using Kalman filters (Miniach and Orlowska-Kowalska, 2025; Xiahou et al., 2017), mathematical differential operators (Das and Manohar, 2023), open-loop estimation techniques (Adamczyk and Orlowska-Kowalska, 2022; Teler et al., 2025b) and observer-based estimators (Azzoug et al., 2020). Concepts based on simple logic and physical relationships are also being investigated (Dybkowski and Jankowska, 2022). Methods that are independent of motor parameters, such as single-phase enhanced phase-locked loop (SEPLL), are also used but require at least one functioning sensor in the measurement system (Zuo et al., 2023b). Typical CSFTC strategies involve three primary steps: fault detection, sensor isolation and control system reconfiguration. For instance, Venghi et al. (2021) demonstrated a system that can diagnose single and multiple CS faults, while Manohar and Das (2017) proposed a method using flux-linkage observers for current estimation. The research spans multiple motor types including induction motors, doubly-fed induction generators and permanent magnet synchronous machines, highlighting the broad applicability of these fault-tolerant control (FTC) techniques. Accurate estimation of currents is important not only to ensure continuous operation of the drive but also for diagnostic reasons, where stator phase current estimators are used as reference signals for fault detection and classification algorithms (Skowron et al., 2023; Teler et al., 2023).

Many of the CSFTC methods are based on a mathematical model of the motor, from which equations describing the appropriate estimation algorithm are derived. Such methods involve the problem of determining machine parameters, which can additionally change during drive operation due, for example, to temperature drift (Romero-Laguna et al., 2024; Zhu et al., 2021). In addition, the mathematical models of electric motors that are commonly known and applied in control theory have been derived under a set of simplifying assumptions, including the use of lumped and time-invariant parameters, the symmetry of stator and rotor windings and the neglect of non-linear magnetic phenomena, such as hysteresis and magnetic saturation (Orlowska-Kowalska, 2003). Since the mathematical model is not perfectly accurate, closed-loop observers of the state variables achieve better accuracy than classical estimators, which do not correct their estimates (open-loop observers).

The literature shows that there are few solutions that combine advanced methods of reconstructing stator phase currents with motor parameter identification that can be implemented directly in the control system. Although there are articles, such as (Zuo et al., 2023a), which focus on developing an accurate mathematical model of the motor, the purpose of such solutions is to simulate the operation of the drive using high-performance computing sources, not to implement the estimators in the control system.

Given the continuing demand for highly accurate current reconstruction algorithms, this article introduces three cost-effective approaches aimed at improving the estimation accuracy of stator phase currents in a PMSM motor drive. The first approach employs the classical mathematical model of the motor, in which the inductance values in the d–q axes are assumed constant and are determined by optimisation using the particle swarm optimisation (PSO) algorithm. The second estimator operates on the basis of identified relationships that describe the flux linkage as a function of current. The third estimator additionally incorporates the dependence of flux linkage on rotor position, thereby accounting for spatial harmonics and, consequently, the specific design characteristics of the motor. The study is organised as follows: in the second chapter, details regarding the estimator models are provided. Chapter 3 focuses on theoretical and practical aspects of the determination of necessary parameters for the used estimator models. Chapter 4 presents an experimental comparison of three different methods of stator current estimation in a PMSM drive. The study is finished with conclusions.

2. Stator Current Estimators

To derive equations describing estimator models, it is first necessary to present a mathematical model of a PMSM motor. The mathematical model of a three-phase PMSM drive is derived from the motor circuit equations (Orlowska-Kowalska, 2003). This model is obtained by making the following simplifying assumptions:

a) three-phase windings are treated as symmetrical,
b) resistance and inductance are considered constant,
c) the phenomenon of saturation and hysteresis of the magnetic circuit is ignored,
d) iron and stator losses are ignored,
e) higher harmonics of the spatial field distribution in the gap are also ignored, and only the fundamental harmonic is taken into account.

The adopted assumptions allow the equations of the machine to be derived in the natural ABC three-phase coordinate system. However, such a model is impractical for control applications, which is why spatial vectors of voltages, currents and associated fluxes are considered, allowing the selected three-phase quantities to be transformed into different coordinate systems. The transformation of the vector from the ABC system to the stationary α–β system is performed using the Clarke transformation and from the α–β system to the rotating dq system using the Park transformation. The motor model in the dq coordinate system rotating synchronously with the rotor's associated vector, taking into account simplifying assumptions, is expressed by the following formulas:

- Stator voltage equations:

$$\begin{cases} u_d = R_s i_d + \dfrac{d\Psi_d}{dt} - \omega_e \Psi_q \\ u_q = R_s i_q + \dfrac{d\Psi_q}{dt} + \omega_e \Psi_d \end{cases} \tag{1}$$

- Flux linkages of stator windings:

$$\begin{cases} \Psi_d = L_d i_d + \Psi_f \\ \Psi_q = L_q i_q \end{cases} \tag{2}$$

- Electromagnetic torque:

$$T_e = \frac{3}{2} p_b \left(\Psi_d i_q - \Psi_q i_d \right) \tag{3}$$

In the above equations u_{dq} and i_{dq} are the stator voltage and current, respectively, in the dq axis, R_s is stator resistance, L_{dq} are inductances in the dq axis, p_b is the number of pole pairs, Ψ_{dq} are flux linkages in the dq axis, Ψ_f is permanent magnet flux, ω_e is the electrical speed equals to $\omega_m p_b$, where ω_m is mechanical speed and T_e is electromagnetic torque.

2.1. Virtual current sensor (VCS)

The mathematical model of the current estimator is derived directly from Eqs (1) and (2). Using the flux linkages Eq. (2) and substituting them into the voltage Eq. (1), the following are obtained after transformations:

$$\begin{cases} \dfrac{di_d}{dt} = \dfrac{1}{L_d} \left(u_d - R_s i_d + \omega_e L_q i_q \right) \\ \dfrac{di_q}{dt} = \dfrac{1}{L_q} \left(u_q - R_s i_q - \omega_e \left(L_d i_d + \Psi_f \right) \right) \end{cases} \tag{4}$$

The above system of equations constitutes the basic model of an open-loop current estimator and will be referred to as VCS (Adamczyk and Orlowska-Kowalska, 2022). The formula contains parameters which, due to simplifying assumptions, are considered constant: resistance R_s, inductance L_{dq} and permanent magnet flux Ψ_f. This model is therefore sensitive to the accuracy of their determination and does not have any correction terms, as is the case with the Luenberger observer. The software implementation of this model can be achieved by using a modified Euler method with a sampling time Δt:

$$\begin{cases} \hat{i}_d^k = \hat{i}_d^{k-1} + \dfrac{\Delta t}{L_d} \left(u_d^{k-1} - R_s \hat{i}_d^{k-1} + \omega_e^{k-1} L_q \hat{i}_q^{k-1} \right) \\ \hat{i}_q^k = \hat{i}_q^{k-1} + \dfrac{\Delta t}{L_q} \left(u_q^{k-1} - R_s \hat{i}_q^{k-1} - \omega_e^{k-1} \left(L_d \hat{i}_d^k + \Psi_f \right) \right) \end{cases} \tag{5}$$

In the above formulas, notation is used in which the superscript k denotes a sample at time $t = k\Delta t$, where $k \in \mathbb{Z}$ and $k - i$ denotes a historical sample from i sampling periods ago. In the above equations, attention should be paid

to the component $L_d\hat{i}_d^k$ appearing in the second equation, which depends on the value $\hat{i}_d^k$ determined in the current calculation step.

2.2. LookUp table-based estimator (LUTE)

The current estimator model presented in the previous subsection is derived from equations that were developed taking into account simplifying assumptions regarding time-invariant parameters, omitting phenomena related to saturation and hysteresis of the magnetic circuit and considering only the fundamental component of the spatial field distribution in the gap. The actual dependence of the flux linkages is generally expressed by a non-linear function of currents i_d and i_q:

$$\begin{cases} \Psi_d = f_d\left(i_d, i_q\right) \\ \Psi_q = f_q\left(i_d, i_q\right) \end{cases} \tag{6}$$

By determining the derivatives composed of the above relationships and substituting them into the voltage Eq. (1), the following system of equations is obtained after appropriate transformations:

$$\begin{cases} \dfrac{di_d}{dt} = \dfrac{1}{\dfrac{\partial \Psi_d}{\partial i_d}}\left(u_d - R_s i_d - \dfrac{\partial \Psi_d}{\partial i_q}\dfrac{di_q}{dt} + \omega_e \Psi_q\right) \\ \dfrac{di_q}{dt} = \dfrac{1}{\dfrac{\partial \Psi_q}{\partial i_q}}\left(u_q - R_s i_q - \dfrac{\partial \Psi_q}{\partial i_d}\dfrac{di_d}{dt} - \omega_e \Psi_d\right) \end{cases} \tag{7}$$

In the above equations, the inductance parameters and the value of the flux from permanent magnets have been replaced by the values of the associated stator flux and its derivatives. This model, therefore, takes into account the actual characteristics of the flux linkages. The open-loop estimator model described above requires knowledge of the relationships Eq. (6) that will be determined by experimental measurements, and the appropriate measurement procedure will be described later in this article. The values obtained from the measurements can then be stored in a look-up table (LUT) and used during the operation of the electric drive controller algorithm. The discrete implementation of this model after applying Euler's method is as follows:

$$\begin{cases} \hat{i}_d^k = \hat{i}_d^{k-1} + \dfrac{\Delta t}{\dfrac{\partial f_d^{k-1}}{\partial i_d}}\left(u_d^{k-1} - R_s \hat{i}_d^{k-1} - \dfrac{\partial f_d^{k-1}}{\partial i_q}\dfrac{\hat{i}_q^{k-1} - \hat{i}_q^{k-2}}{\Delta t} + \omega_e^{k-1} f_q^{k-1}\right) \\ \hat{i}_q^k = \hat{i}_q^{k-1} + \dfrac{\Delta t}{\dfrac{\partial f_q^{k-1}}{\partial i_q}}\left(u_q^{k-1} - R_s \hat{i}_q^{k-1} - \dfrac{\partial f_q^{k-1}}{\partial i_d}\dfrac{\hat{i}_d^{k-1} - \hat{i}_d^{k-2}}{\Delta t} - \omega_e^{k-1} f_d^k\right) \end{cases} \tag{8}$$

where ^ indicates estimated values and $f_d^k = f_d\left(\hat{i}_d^k,\ \hat{i}_q^{k-1}\right)$, $f_d^{k-1} = f_d\left(\hat{i}_d^{k-1},\ \hat{i}_q^{k-1}\right)$, $f_q^{k-1} = f_q\left(\hat{i}_d^{k-1},\ \hat{i}_q^{k-1}\right)$.

2.3. Extended lookup table-based estimator (ELUTE)

Further development of the estimator model involves taking into account the dependence of the stator flux not only on currents but also on the rotor position:

$$\begin{cases} \Psi_d = F_d\left(i_d, i_q, \theta\right) \\ \Psi_q = F_q\left(i_d, i_q, \theta\right) \end{cases} \tag{9}$$

The estimator equations currently take the following form:

$$\begin{cases} \dfrac{di_d}{dt} = \dfrac{1}{\dfrac{\partial \Psi_d}{\partial i_d}}\left(u_d - R_s i_d - \dfrac{\partial \Psi_d}{\partial i_q}\dfrac{di_q}{dt} - \dfrac{\partial \Psi_d}{\partial \theta}\dfrac{d\theta}{dt} + \omega_e \Psi_q \right) \\ \dfrac{di_q}{dt} = \dfrac{1}{\dfrac{\partial \Psi_q}{\partial i_q}}\left(u_q - R_s i_q - \dfrac{\partial \Psi_q}{\partial i_d}\dfrac{di_d}{dt} - \dfrac{\partial \Psi_q}{\partial \theta}\dfrac{d\theta}{dt} - \omega_e \Psi_d \right) \end{cases} \tag{10}$$

The difference between the LUTE estimator Eq. (7) and the above equation concerns the presence of an additional term that takes into account changes in the flux from the position. As before, these values are tabulated, and the discrete equation after applying the Euler method is as follows:

$$\begin{cases} \hat{i}_d^k = \hat{i}_d^{k-1} + \dfrac{\Delta t}{\dfrac{\partial F_d^{k-1}}{\partial i_d}}\left(u_d^{k-1} - R_s \hat{i}_d^{k-1} - \dfrac{\partial F_d^{k-1}}{\partial i_q}\dfrac{\hat{i}_q^{k-1} - \hat{i}_q^{k-2}}{\Delta t} - \dfrac{\partial F_d^{k-1}}{\partial \theta}\omega_m^{k-1} + \omega_e^{k-1} F_q^{k-1} \right) \\ \hat{i}_q^k = \hat{i}_q^{k-1} + \dfrac{\Delta t}{\dfrac{\partial F_q^{k-1}}{\partial i_q}}\left(u_q^{k-1} - R_s \hat{i}_q^{k-1} - \dfrac{\partial F_q^{k-1}}{\partial i_d}\dfrac{\hat{i}_d^{k-1} - i_d^{k-2}}{\Delta t} - \dfrac{\partial F_q^{k-1}}{\partial \theta}\omega_m^{k-1} - \omega_e^{k-1} F_d^{k} \right) \end{cases} \tag{11}$$

where the derivative of the angular position is replaced by mechanical speed ω_m and $F_d^k = F_d\left(\hat{i}_d^k,\ \hat{i}_q^{k-1}, \theta^{k-1}\right)$, $F_d^{k-1} = F_d\left(\hat{i}_d^{k-1},\ \hat{i}_q^{k-1}, \theta^{k-1}\right)$, $F_q^{k-1} = F_q\left(\hat{i}_d^{k-1},\ \hat{i}_q^{k-1}, \theta^{k-1}\right)$.

2.4. FOC with current estimator

The verification of each of the three estimators was carried out in the FOC structure with a fixed power angle $\delta = \pi / 2$, which is equivalent to forcing the current $i_d = 0$. In this case, the equation for electromagnetic torque Eq. (3) is simplified and, assuming a constant flux value, indicates a linear relationship between electromagnetic torque and motor current:

$$T_e = \frac{3}{2} p_b \Psi_d i_q \tag{12}$$

The control structure using previously developed current estimator models is presented in Figure 1. The tests were first conducted for control using measurements from CS, and then switch was changed to check the operation of the system using estimated current values. During the operation of the system on the physical measurements from the CS, estimated signals were also recorded. In this way, it is possible to compare the quality of estimation under default drive operating conditions, i.e., using measurements from sensors, and under closed-loop control conditions, when the estimated values affect the operation of the drive.

3. Identification of Necessary Parameters

3.1. Inverter commissioning (IC)

Each current estimator model presented in the previous chapter includes voltage and velocity measurements in its equations. The accuracy of measuring these physical quantities will directly affect the estimator's performance, assuming that the other parameters have been correctly identified. This subsection will discuss the problem of voltage measurement.

The electric drive system includes a voltage inverter, which is treated as an ideal voltage amplifier when designing the control algorithm. However, the output voltage characteristic of the inverter is non-linear and is affected by dead time effects, commutation delays, voltage drops across power devices, and equivalent resistance and capacitance in the inverter legs. The voltage used in calculations related to the estimation of any physical quantity or in the drive parameter identification procedure can be reproduced on the basis of inverter duty-cycle commands from the control structure and DC bus voltage measurement. If this solution is chosen, the control structure must include

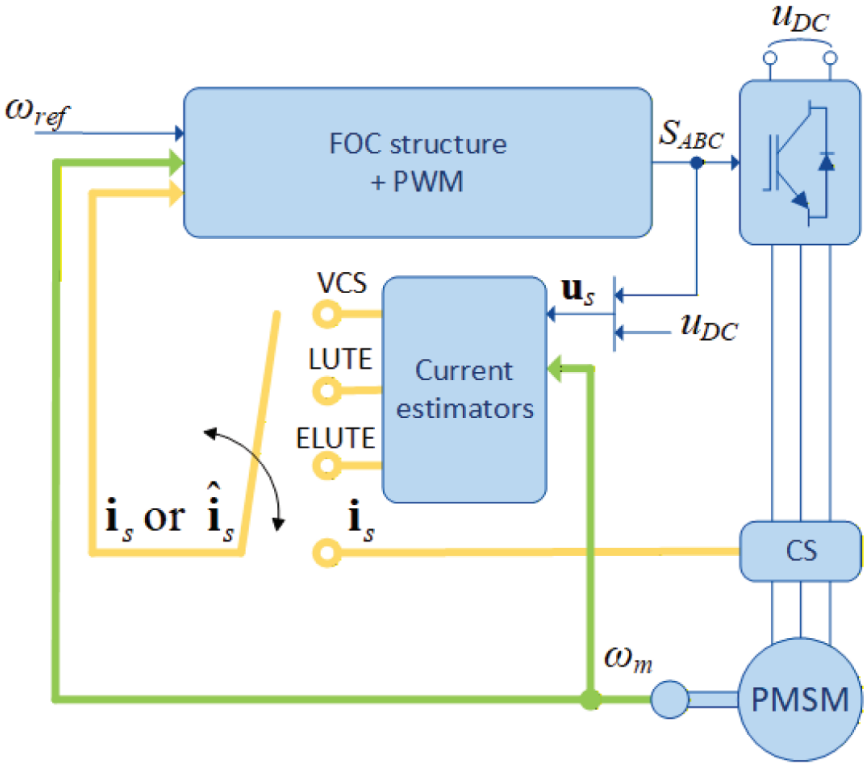

Figure 1. Scheme of control structure under study. CS, current sensors; ELUTE, extended lookup table-based estimator; FOC, field oriented control; LUTE, lookup table-based estimator; VCS, virtual current sensor.

an appropriate algorithm for compensating for the inverter's dead time. Compensation for this phenomenon is important for drives with sensorless control, as voltage distortions have a significant impact on the operation of the estimation or identification algorithm, especially at low drive speeds.

Compensation of non-linear inverter phenomena is based on determining the parameters of the mathematical model of the inverter (identification stage) and then using these parameters to calculate the compensating voltage added to the reference voltages in the control structure (compensation stage).

The selected process for identifying inverter parameters involves performing a series of measurements in a system with deactivated compensation using a vector drive control structure (Bedetti et al., 2015). The voltage needed to maintain the reference current value is the result of the action of the controllers, and in the steady state, it corresponds to the sum of the voltage drop across the resistance of the wires and the voltage distorted by the inverter. Thus, by forcing a step current waveform, the corresponding value of the reference voltage from the regulators can be read. Based on the obtained voltage characteristics as a function of current, it is then possible to determine the total resistance of the motor stator windings and wires R_s, as well as the parameters required for compensation, which include the dead time T_{DT} and the equivalent capacitance in the inverter leg C_{out}. The process involves comparing the obtained characteristics with the mathematical model of the inverter, and the resulting parameters can then be used in the dead time compensation process.

Voltage and current measurements in the identification stage and in the compensated system, taken on the test bench, are shown in Figure 2.

The determined parameter values in the identification process are: $R_s^{\mathrm{IC}} = 1.32\Omega$, $C_{\mathrm{out}}^{\mathrm{IC}} = 1.47\,\mathrm{nF}$ and $T_{\mathrm{DT}}^{\mathrm{IC}} = 3.91\,\mu\mathrm{s}$, where superscript IC stands for inverter commissioning. Figure 2 shows an example point (i_A, u_A), for which the resistance value is $R_s^{i_A,u_A} = \frac{u_A}{i_A} = \frac{5.4V}{4A} = 1.35\Omega$. This value is comparable to the identified resistance value R_s at the identification stage $\left(R_s^{\mathrm{IC}} = 1.32\Omega\right)$, which means that the reference voltage from the control structure needed to force the set current value is only the voltage drop across the resistance. The estimator models do not take into

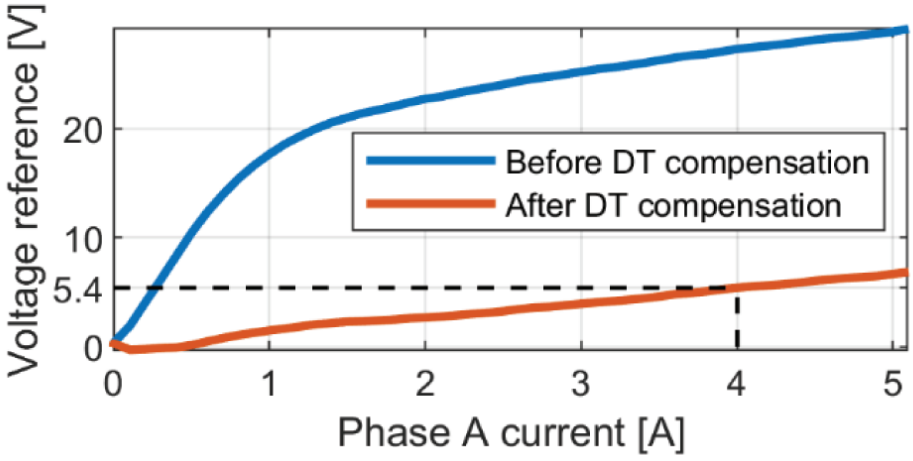

Figure 2. Measurements of current vs. voltage before and after compensation of inverter distortions.

account the inverter, ignoring voltage drops across power electronic devices, so any non-linearities in the real system will degrade the performance of the estimator. Inaccurate estimation of dead time will manifest itself in non-linear current-voltage characteristics, reducing the performance of the estimator. This confirms the validity and effectiveness of the inverter dead-time compensation method used in the context of developing an accurate estimator of the stator currents of the motor under study.

3.2. Speed measurements

Estimator models require speed measurements in addition to voltage measurements. During the course of the work, it turned out that the use of any type of speed filter reduces the quality of the estimator's performance. Regardless of how the speed is determined for the control structure and how it is filtered, the estimator model requires knowledge of the exact speed value, which does not show any phase shift. It is therefore proposed to determine the speed as a derivative of the position calculated using numerical methods. In this case, Savitzky–Golay filter was used (Savitzky and Golay, 1964). The method involves a local approximation of m consecutive signal samples with an nth-degree polynomial using the least squares method, followed by analytical determination of the derivative value at the centre point of the window. The following method with a sampling time Δt was used in the conducted research, which uses a quadratic polynomial ($n = 2$) and $m = 7$ samples:

$$\frac{d\theta^k}{dt} = \omega_m^k \approx \frac{1}{28\Delta t}\left[-3\theta^{k-3} - 2\theta^{k-2} - \theta^{k-1} + \theta^{k+1} + 2\theta^{k+2} + 3\theta^{k+3}\right] \tag{13}$$

The formula above uses only six samples because the corresponding coefficient for θ^k at the centre point of the window is equal to zero. In calculations related to estimators, instead of the values of velocity ω_m^{k-1} and ω_e^{k-1} in formulas (5), (8) and (11), a derivative calculated for a sample delayed by three computational steps was used, thus compensating for the unknown future measurements. Such a small delay is of little significance given the considerable inertia of the system. However, in the case of a very long measurement acquisition period, this should be taken into account.

It should also be mentioned that the Savitzky–Golay filter can be designed for a time window length other than the one presented, and the point for which the derivative is calculated does not have to be in the centre of the time window, as is the case here. Shifting this point allows only historical time samples to be used. However, this approach amplifies measurement noise in relation to the method presented above, which results directly from the interpretation of the differentiating operator Eq. (13) as an FIR filter (Hamming, 1989).

3.3. VCS parameters

In the equation of the mathematical model of the VCS estimator appear the values of resistance R_s and inductance L_{dq}, as well as the value of the permanent magnets' flux Ψ_f. The purpose of the ongoing research is to develop

an algorithm that will provide an accurate reproduction of the current values. For this reason, it was decided to select the parameters of the mathematical model of the estimator through an optimisation process. Measurements were carried out on a test bench with a PMSM motor for 25 different operating points (10%, 25%, 50%, 75% and 100% of the rated speed and 0%, 25%, 50%, 75% and 100% of the rated torque). The parameters R_s, L_{dq} and Ψ_f of the VCS model were then determined by minimising the objective function E using the PSO algorithm. One of the publications on the use of PSO for estimating PMSM motor parameters can be found in Liu et al. (2008). More recent publications with numerous improvements also confirm the effectiveness of the PSO method (Liu et al., 2018). The objective function was defined as the mean squared error between the currents recorded on the test bench and the estimated currents:

$$E = \frac{1}{n}\sum_{k=1}^{n}\left[\left(\hat{i}_d(k) - i_d(k)\right)^2 + \left(\hat{i}_q(k) - i_q(k)\right)^2\right] \tag{14}$$

where n denotes the number of all recorded measurements. The calculations performed for each particle in the swarm were based on the determination of the value of the estimated current according to Eq. (4), followed by the calculation of the error E for the entire set of measurement data. Minimisation of the error E was done by updating the positions of individual particles in the swarm, which represented the set of parameters R_s, L_{dq} and Ψ_f. The PSO algorithm from the MATLAB environment library was used, in which the swarm size was set to 50 particles and the maximum number of iterations was set to 100. The remaining parameters were left as default. During the optimisation, the assumption of equal inductance $L_d = L_q$ was made. The parameters obtained from the optimisation process were: $R_s^{\mathrm{PSO}} = 1.38\,\Omega$, $L_d^{\mathrm{PSO}} = L_q^{\mathrm{PSO}} = 39.7\,\mathrm{mH}$, $\Psi_f^{\mathrm{PSO}} = 0.3484\,\mathrm{V\cdot s}$. The algorithm was run three times, and each time the results were identical, with the calculation time taking <4 min on a computer with an Intel i5-12500H processor. The parameters were then used in the estimation algorithm of the currents on the test bench. It should be noted that the resistance values obtained from optimisation $R_s^{\mathrm{PSO}} = 1.38\,\Omega$ and from the inverter identification process $R_s^{\mathrm{IC}} = 1.32\,\Omega$ are roughly the same, which indicates that both processes are correct.

3.4. LUTE parameters

Determining the dependence of flux as a function of current is among the basic methods of identifying synchronous motors. The mathematical model obtained in this process, which takes into account the magnetic characteristics of the motor, is used in the design process and accurate control. Experimental methods for determining this motor model can be divided into locked-rotor and constant-speed methods. The method that makes it possible to determine the magnetic characteristics of any synchronous motor involves running the machine under test to a constant speed and then forcing currents to flow in a synchronous d–q coordinate system using a vector control structure. Based on the measurements of currents, voltages and speed, the value of the flux at the tested operating point can be determined.

The chosen method for identifying a non-linear model of a PMSM motor is to test the machine at a fixed operating point (Armando et al., 2013). In this case, the fluxes for a given current i_{dq} can be determined from Eq. (1) by neglecting the flux derivatives, thus obtaining:

$$\begin{cases} \Psi_d = \dfrac{u_q - R_s i_q}{\omega_e} \\ \Psi_q = \dfrac{-\left(u_d - R_s i_d\right)}{\omega_e} \end{cases} \tag{15}$$

Calculating the flux-linkages using above equation requires accurate voltage measurements and determination of resistance R_s. These conditions are met by using dead-time compensation according to the algorithm presented in subsection 3.1. of this article. However, accuracy of the resistance determination is less important in this case because procedure is performed in such a way that uncertainties of R_s are compensated. This requires recording data in motoring and braking modes of operation of the drive by forcing current vector of $\left(i_d^{\mathrm{ref}} + j i_q^{\mathrm{ref}}\right)$ then $\left(i_d^{\mathrm{ref}} - j i_q^{\mathrm{ref}}\right)$ and again $\left(i_d^{\mathrm{ref}} + j i_q^{\mathrm{ref}}\right)$. During the measurements, it was assumed that the working point grid would consist of 522 points (i_d^{ref} from −8 A to 0.5 A with 0.5 A step and i_q^{ref} from 0 A to 14 A with 0.5 step). Since average value of flux in steady-state is of interest, then all measurements must be averaged over at least one mechanical period, thus

eliminating unwanted signal components. During testing, the motor maintains a constant speed which should be about 1/3 of the rated speed. Such a speed is a compromise between low iron losses and high back-electromotive force. Taking into account all these requirements the flux-linkages can be calculated with:

$$\begin{cases} \Psi_d = \dfrac{\frac{1}{2}\left(\frac{u_{q1}+u_{q3}}{2}+u_{q2}\right)}{\omega_e} \\ \Psi_q = \dfrac{-\frac{1}{2}\left(\frac{u_{d1}+u_{d3}}{2}-u_{d2}\right)}{\omega_e} \end{cases} \tag{16}$$

where indexes 1, 2 and 3 correspond to motoring, braking and motoring mode, respectively. The derivatives of flux with respect to current required in the non-linear estimator model Eq. (7) can be easily determined using numerical differentiation methods and are also functions of current. The magnetic model obtained in this way (Figure 3) is stored in the controller memory using a lookup table (LUT) and used in the LUTE estimator calculations.

3.5. ELUTE parameters

The flux maps obtained in the previous subsection are average values determined in a steady state. However, the actual flux contains higher harmonics of the spatial distribution of the field in the gap. Taking into account the additional dependence of the flux on the angular position of the rotor requires the use of the procedure described by Bojoi et al. (2024), which is an extension of the procedure described in the previous section. Based on measurements in a steady state, the flux value is determined for different rotor positions, making it possible to accurately reproduce the flux-current relationships characterising the tested motor. During the calculations, it was assumed that the resolution with which the fluxes were calculated was 1°, so 360° values were obtained for each operating point. As with the previous method, the determined relationships are recorded and stored in a LUT table for future use in ELUTE calculations. Figure 4 shows example flux maps for a position angle of 0°, while Figure 5 shows the

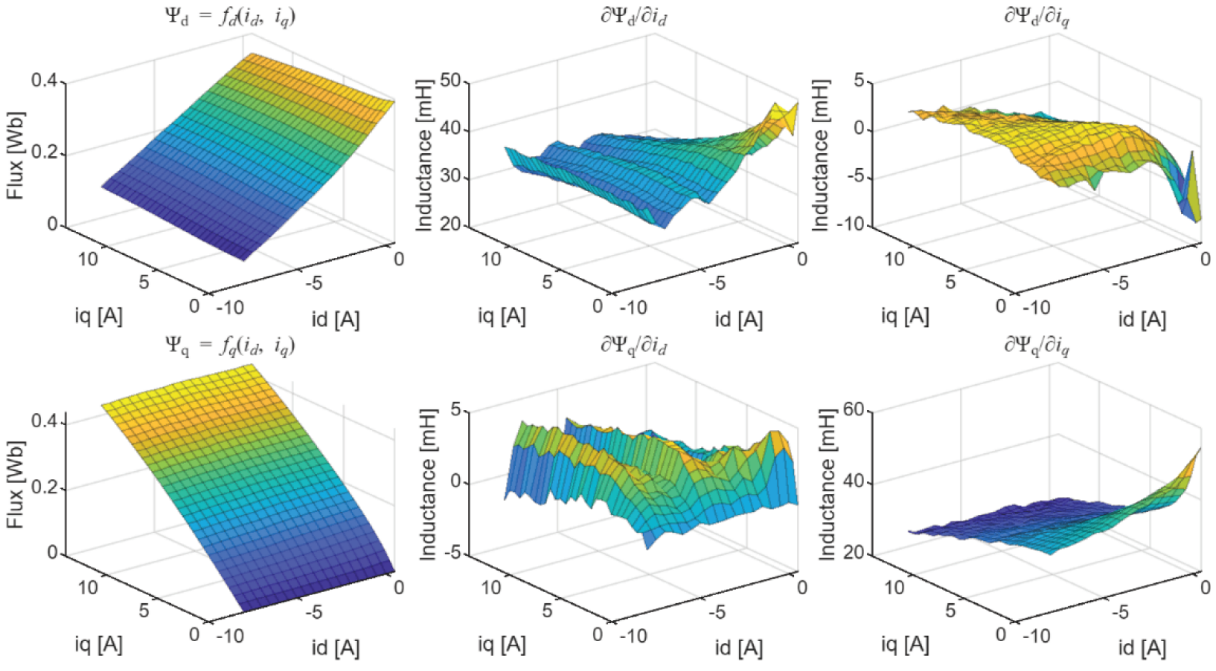

Figure 3. Magnetic model of the PMSM under study used in LUTE. LUTE, lookup table-based estimator.

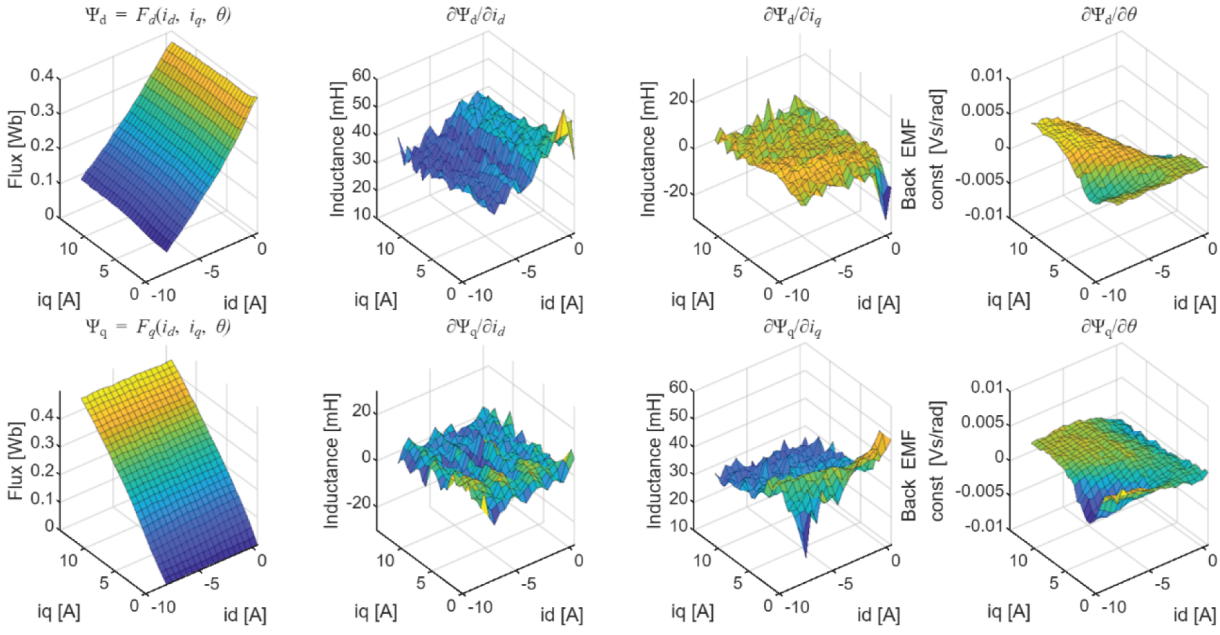

Figure 4. Extended magnetic model for PMSM under study for rotor position $\theta = 0$ deg.

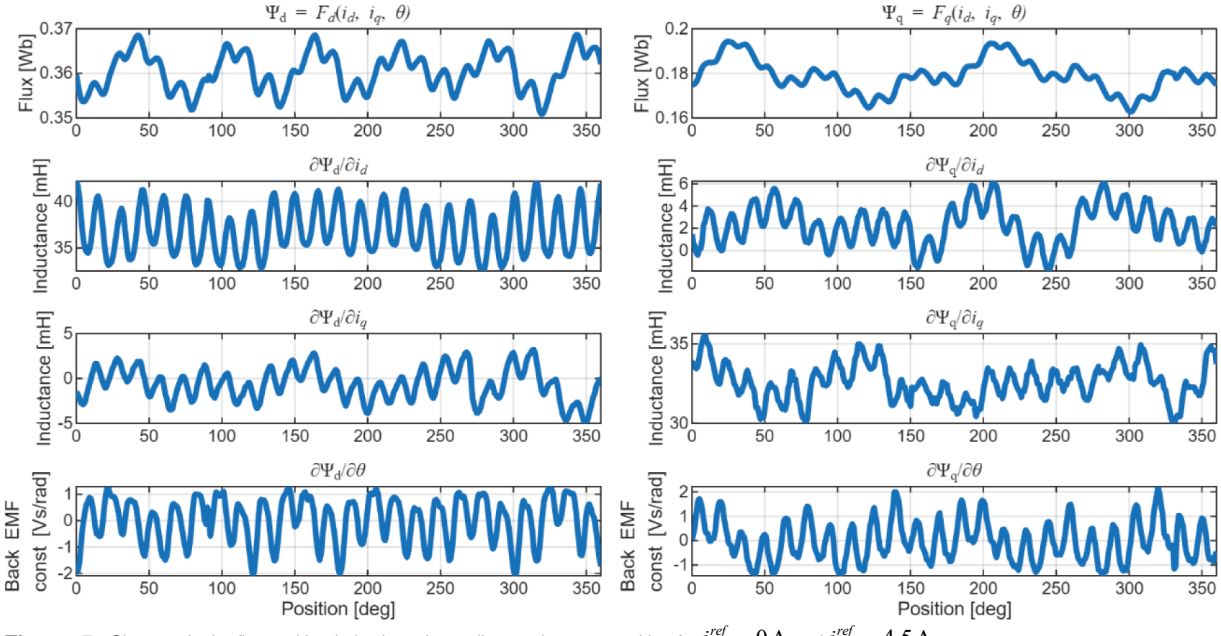

Figure 5. Changes in the flux and its derivatives depending on the rotor position for $i_d^{ref} = 0\,\mathrm{A}$ and $i_d^{ref} = 4.5\,\mathrm{A}$.

waveforms of the determined values for a selected operating point depending on the position angle. The curves of the analysed quantities in Figure 5 show relatively high variability across the entire range of rotor position angles, which manifests itself in irregular surfaces in Figure 4. By computing the mean values of the waveforms presented in Figure 5 and subsequently plotting these values as a function of the operating point, the characteristics similar to the shown in Figure 3 are obtained. The variations in the mean values are less pronounced across different operating points; therefore, the resulting surfaces exhibit a smoother profile.

4. Experimental Results and Discussion

4.1. Laboratory setup

The experimental test bench (Figure 6) consisted of a Lenze MCS14H15 PMSM-controlled motor with a power output of 2.5 kW, a rated speed of 1,500 *r*/min and a rated current of 6.6 A supplied from a frequency converter of custom design and a 4 kW induction motor operating as a load and supplied from a TWERD 5.5 kW industrial inverter. The PMSM motor operated according to the idea of FOC with a constant power angle, meaning that the reference current i_d was zero. The control system compensated for the inverter's dead time according to the algorithm presented in subsection 3.1. The measurement system consisted of a set of LEM LA 55-P sensors and a resolver mechanically coupled to the PMSM motor rotor.

The measurements used in the studies on the optimisation of VCS parameters with PSO and the verification of the operation of all estimators were carried out for 25 different operating points (10%, 25%, 50%, 75% and 100% of the rated speed and 0%, 25%, 50%, 75% and 100% of the rated torque). Waveforms of the reference speeds and load torques are shown in Figure 7.

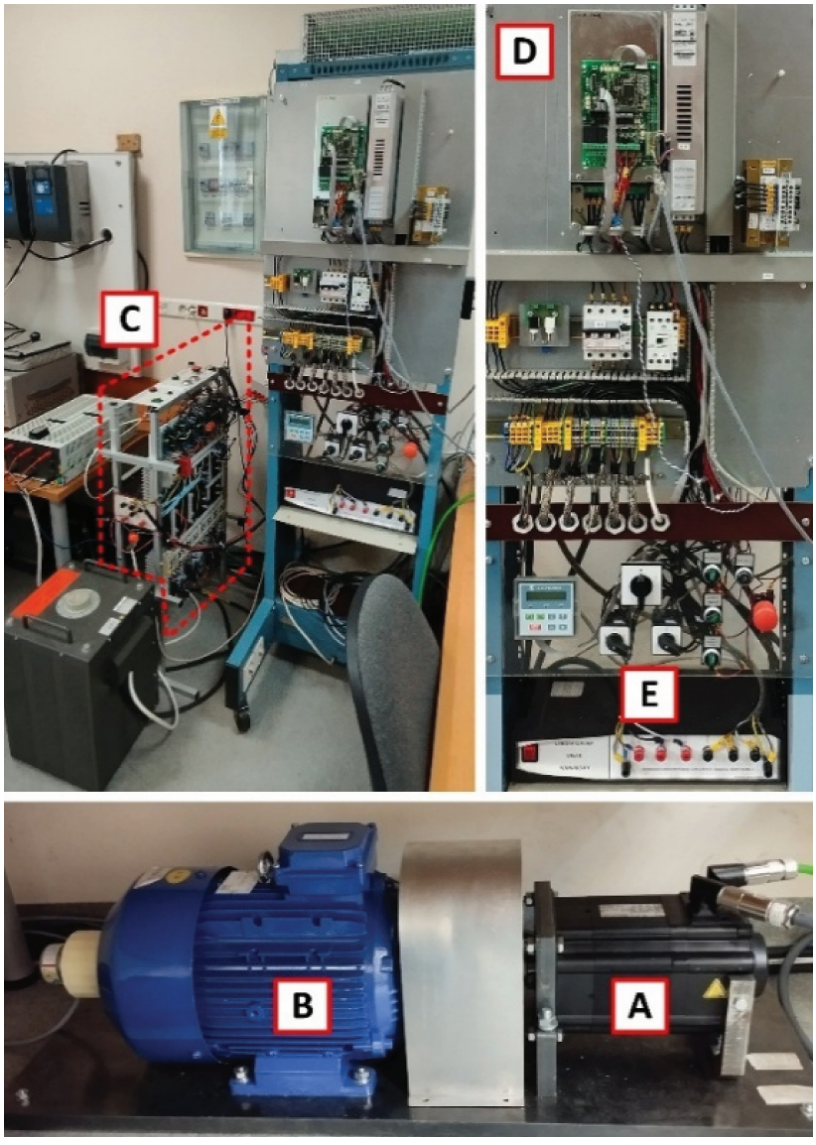

Figure 6. Experimental setup. (a) PMSM motor under study, (b) load motor (induction machine), (c) frequency inverter (control of PMSM), (d) TWERD frequency inverter (control of the load) and (e) measurement system for stator currents and DC-bus voltage of the PMSM drive.

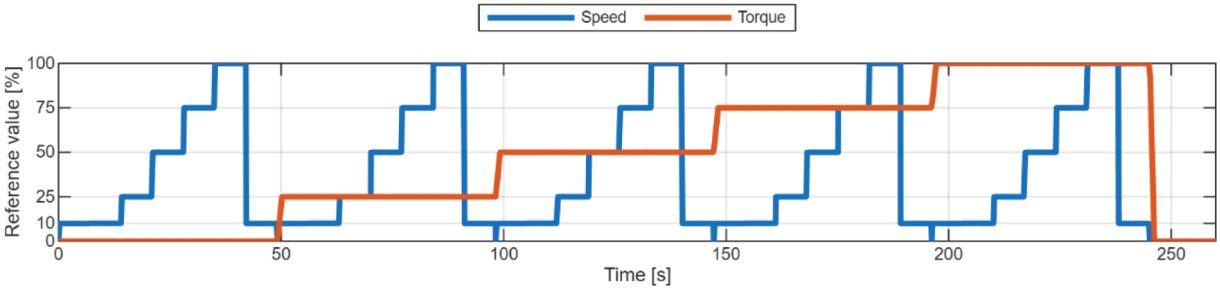

Figure 7. Reference speed and torque used during research.

4.2. Performance analysis of estimator models

Two scenarios were considered in this study. In the first scenario, the control structure relied on measurements from CS, while the estimators did not influence the control. Nevertheless, the estimated values by all three methods were recorded, and this mode of operation is designated as the current sensor control loop (CSCL). In the second scenario, one of the estimators was incorporated into the control loop, and the structure used only estimated currents to determine the control signals. The measured currents, therefore, had no effect on the operation of the drive. In this case, both the current estimated by the selected estimator and the current measured by the sensors were recorded, even though the sensors had no influence on the control structure. This mode of operation is referred to as the sensorless control loop (SCL).

The example of recorded current waveforms for CSCL and SCL is shown in Figures 8 and 9. The waveforms show that the average values of the VCS for the SCL differ significantly from the measured currents. For rated speed and load, VCS and LUTE average the current value, thus not reflecting the actual waveform. The ELUTE appears to be the most accurate, as it reflects the local current dynamics.

For both scenarios (CSCL and SCL), steady states were extracted and the root mean square error (RMSE) of the estimation for every operating point was calculated according to the formula:

$$RMSE = \sqrt{\frac{1}{N}\sum_{k=1}^{N}\left[\left(i_{d,k} - \hat{i}_{d,k}\right)^2 + \left(i_{q,k} - \hat{i}_{q,k}\right)^2\right]} \tag{17}$$

By using the above formula, the estimation error is characterised by a single factor, which further describes the accuracy of the estimation depending on the operating point of the drive. The RMSE values for all 25 operating points for CSCL and SCL are shown, respectively, in Figures 10 and 11. It can be seen that VCS has the largest error of all three estimators, while ELUTE has the smallest. The improvement in the quality of ELUTE estimation compared to LUTE is small but noticeable. For the LUTE and ELUTE estimators, an increase in RMSE is also visible with increasing drive speed. RMSE for VCS appears to be smallest for a 50% load, which will be discussed in more detail later in the article. A summary of the estimation quality for all methods is provided in Table 1, which shows the average RMSE calculated from the RMSE values for all tested drive operating points, together with the median, minimum and maximum values, range calculated as maximum minus minimum and standard deviation.

The quality of current reproduction was determined based on the correlation between measured and estimated currents in SCL (Figure 12). Based on Pearson's correlation coefficient denoted as r, the ELUTE estimator can be selected as the best, but the difference in the coefficient for LUTE is not significant. The VCS estimator performs by far the worst, as its fixed model parameters do not work across the entire range of speeds and loads. However, referring to previous conclusions, it can be noted that in the area corresponding to 50% load, the estimated currents best fit the currents measured for VCS. This is due to the optimisation process of the parameters of this model, which were selected in such a way as to minimise the error between currents across the entire range of speeds and loads. This corresponds to the averaging effect of the model parameters and thus explains why the RMSE of the estimation is smallest at this operating point (see Figures 10 and 11).

The impact of the selected estimator operating in the control loop was examined by determining the total harmonic distortion (THD) coefficient for the current measured by CS in phase A. The results are presented in relation to the drive operating point in Figure 13, where CSCL is the reference point of THD, and VCS, LUTE and ELUTE refer to the THD calculated for the SCL. Taking into account speeds in the range up to 75% of the rated

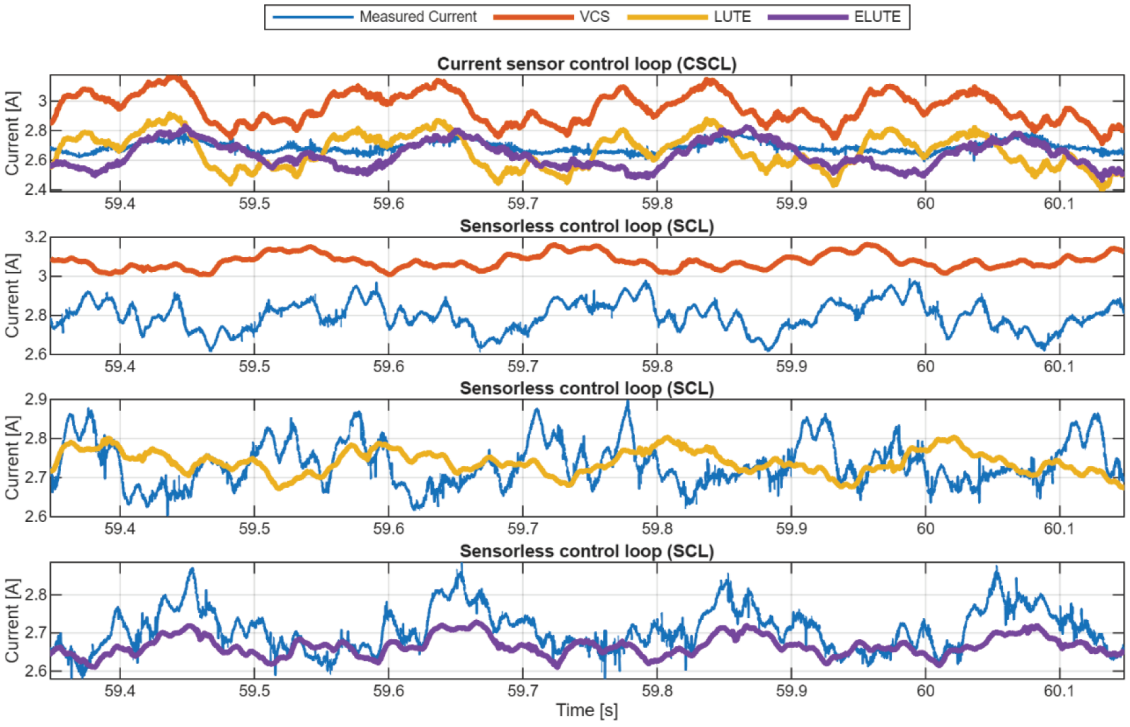

Figure 8. Waveforms of i_q current for different estimation methods (10% of nominal speed and 25% of nominal load). CSCL, current sensor control loop; ELUTE, extended lookup table-based estimator; LUTE, lookup table-based estimator; SCL, sensorless control loop; VCS, virtual current sensor.

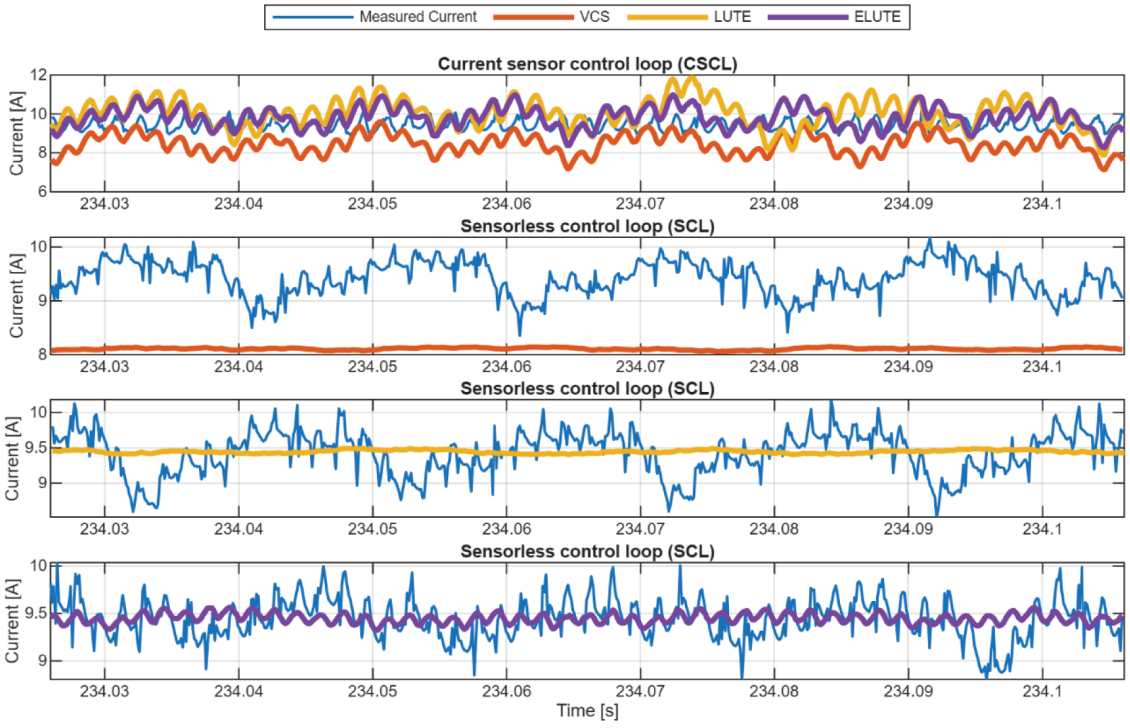

Figure 9. Waveforms of i_q current for different estimation methods (100% of nominal speed and 100% of nominal load). CSCL, current sensor control loop; ELUTE, extended lookup table-based estimator; LUTE, lookup table-based estimator; SCL, sensorless control loop; VCS, virtual current sensor.

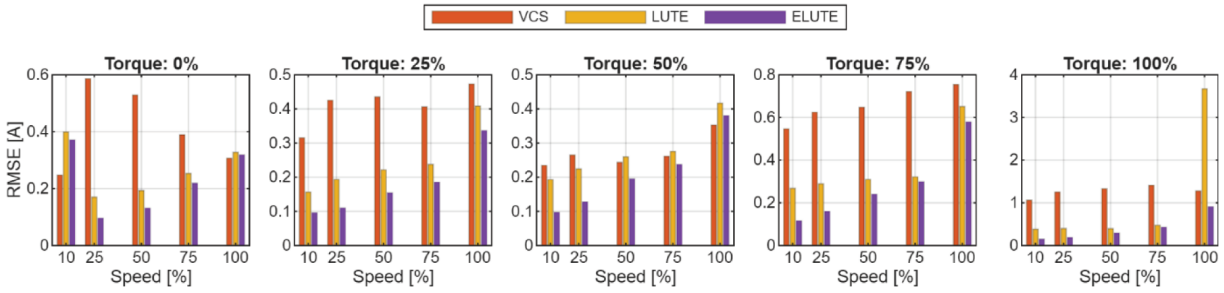

Figure 10. RMSE across operating points of the drive for estimation methods in CSCL. CSCL, current sensor control loop; ELUTE, extended lookup table-based estimator; LUTE, lookup table-based estimator; RMSE, root mean square error; VCS, virtual current sensor.

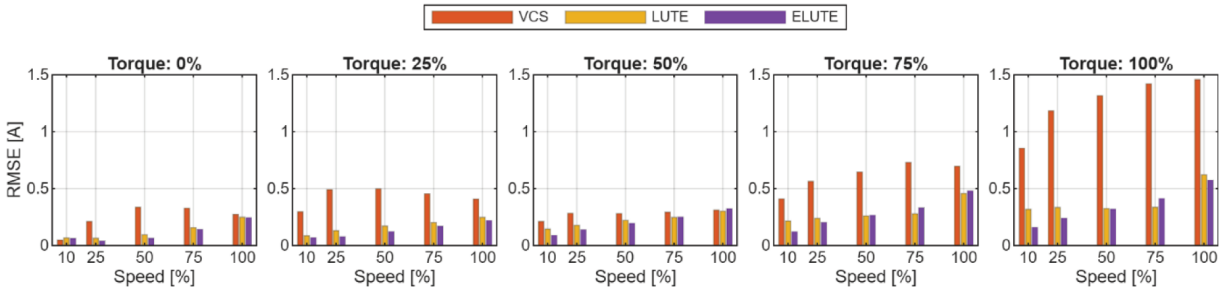

Figure 11. RMSE across operating points of the drive for estimation methods in SCL. ELUTE, extended lookup table-based estimator; LUTE, lookup table-based estimator; RMSE, root mean square error; SCL, sensorless control loop; VCS, virtual current sensor.

Table 1. Statistics of RMSE for estimation methods calculated from all operating points of the drive.

	CSCL						SCL					
Method	Mean	Median	Min	Max	Std	Range	Mean	Median	Min	Max	Std	Range
VCS	0.603	0.473	0.234	1.407	0.372	1.172	0.560	0.409	0.047	1.458	0.396	1.411
LUTE	0.443	0.289	0.156	3.668	0.681	3.512	0.237	0.238	0.064	0.622	0.125	0.558
ELUTE	0.256	0.195	0.095	0.905	0.182	0.809	0.211	0.194	0.039	0.572	0.136	0.533

CSCL, current sensor control loop; ELUTE, extended lookup table-based estimator; LUTE, lookup table-based estimator; RMSE, root mean square error; SCL, sensorless control loop; VCS, virtual current sensor.

speed, regardless of the load, the use of the ELUTE estimator was characterised by the lowest THD value among the three estimators tested. The superiority of ELUTE over other estimators is clearly visible with increasing load. Often, the THD for the SCL was comparable to that of the CSCL. Interesting observations concern increasing THD with increasing speed in the CSCL. However, the use of either estimator reduces the THD at nominal speed in the SCL compared to the CSCL.

4.3. Discussion on CS FTC

An important aspect of the estimators discussed is their applicability in the FTC system for detecting CS faults. Fault detection methods are usually based on determining the residuum between the measured and estimated currents in CSCL mode. In this case, the control structure uses the measurements from the CS in the drive system for control, and the current estimator serves as a reference model for the process. If the residuum calculated in the simplest case as the difference between the currents exceeds the set detection threshold, then the system should be switched to SCL mode. For this reason, it is necessary for the estimator to reproduce the measured currents as accurately as possible. A detailed examination of the estimation quality for changing drive operating points is illustrated in Figures 14 and 15, which shows histograms of the estimation error (residuum) calculated as:

$$error = \sqrt{\left(i_d^2 + i_q^2\right)} - \sqrt{\left(\hat{i}_d^2 + \hat{i}_q^2\right)} \tag{18}$$

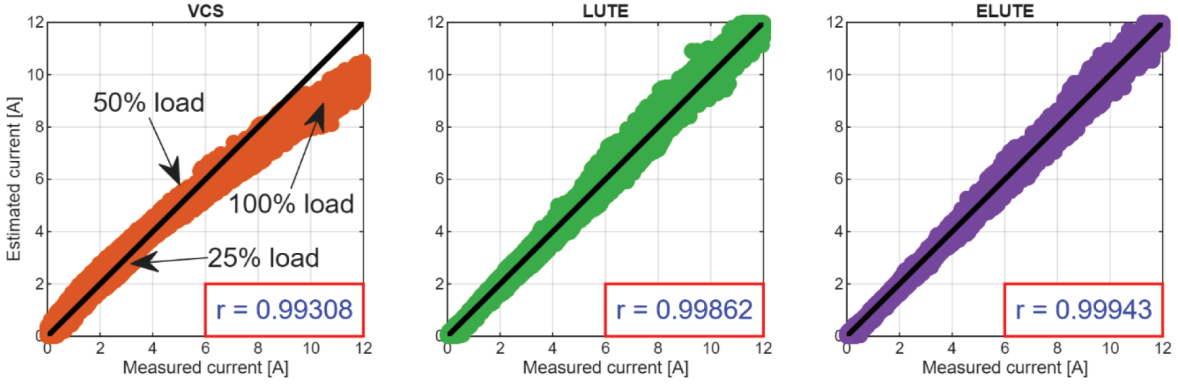

Figure 12. Correlations between measured and estimated current in the SCL for estimation methods under study. ELUTE, extended lookup table-based estimator; LUTE, lookup table-based estimator; SCL, sensorless control loop; VCS, virtual current sensor.

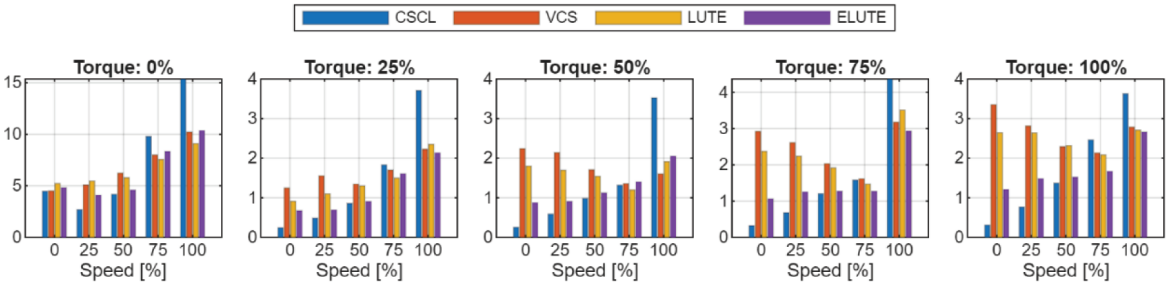

Figure 13. THD calculated for phase A current for CSCL and SCL with different estimation methods. CSCL, current sensor control loop; ELUTE, extended lookup table-based estimator; LUTE, lookup table-based estimator; SCL, sensorless control loop; THD, total harmonic distortion; VCS, virtual current sensor.

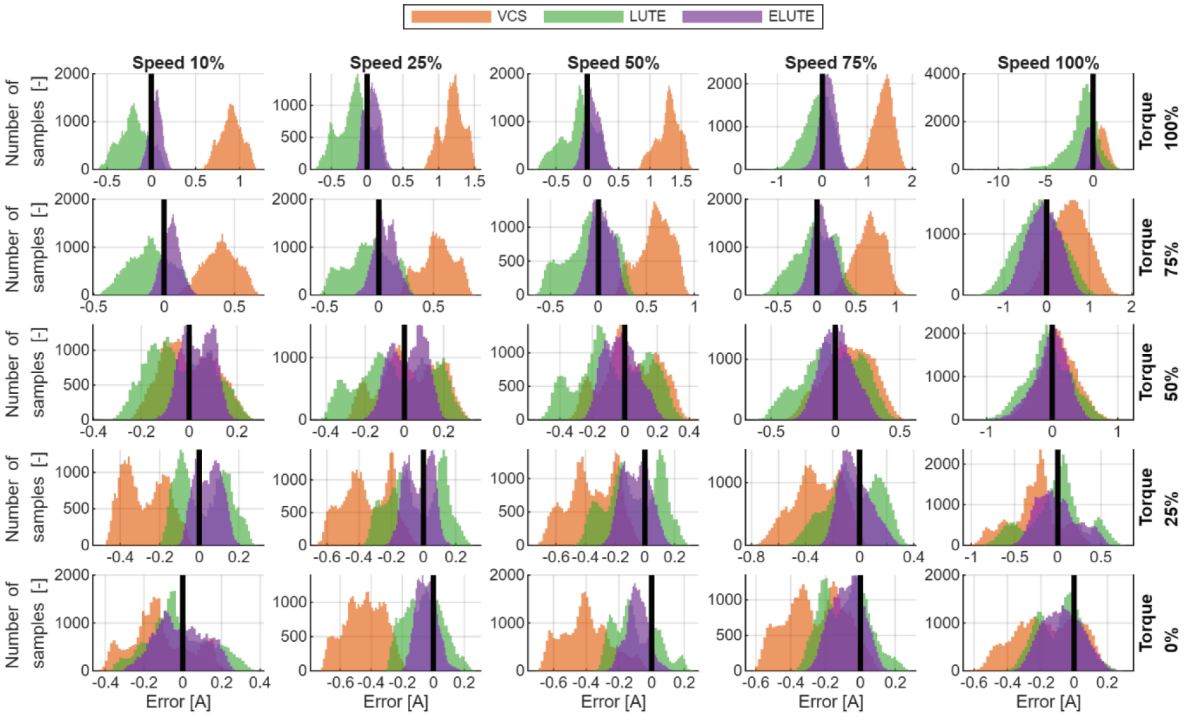

Figure 14. Histograms of the estimation error for CSCL for different PMSM operating points. CSCL, current sensor control loop; ELUTE, extended lookup table-based estimator; LUTE, lookup table-based estimator; VCS, virtual current sensor.

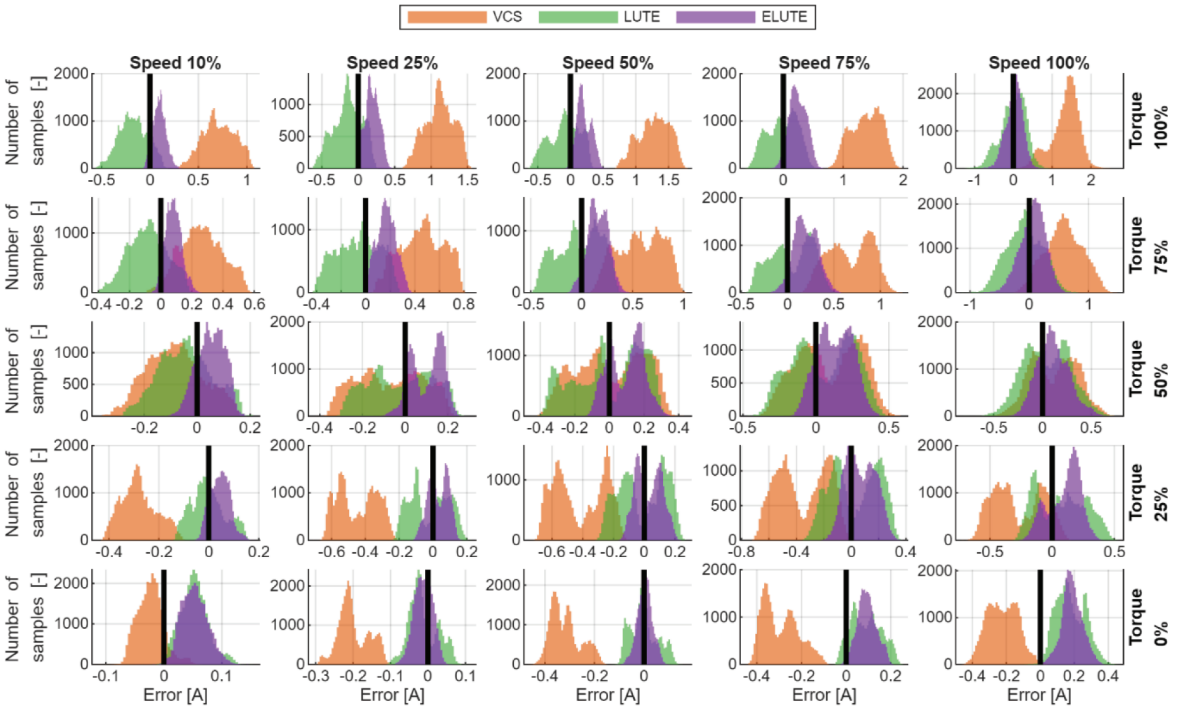

Figure 15. Histograms of the estimation error for SCL for different PMSM operating points. ELUTE, extended lookup table-based estimator; LUTE, lookup table-based estimator; SCL, sensorless control loop; VCS, virtual current sensor.

In the case of the ELUTE estimator, the data spread is the smallest regardless of the operating point, which suggests that the estimation accuracy is therefore the best among the estimators tested. Based on the histograms shown in Figure 14, it can be seen that when using VCS, it is very difficult to define the detection threshold because, depending on the operating point of the drive, the average error is not zero. The use of LUTE or ELUTE estimators in the context of fault detection would be possible, but the adaptive detection threshold would be preferable. This conclusion is a future research direction that should be investigated.

5. Conclusions

This study presents three current estimators derived from a mathematical model of a PMSM motor. They differ in the way the stator flux is described. The VCS model uses a linear dependence of flux linkages with time-constant resistance and inductance parameters. The LUTE model takes into account the actual characteristics of the flux as a function of current determined for the steady state, but only considering the fundamental harmonic. The ELUTE model extends these characteristics to include dependence on the rotor position, thus taking into account spatial harmonics.

The use of any of the estimators requires reliable voltage and speed measurements. This condition can be met by appropriate dead time compensation, thanks to which the reference voltage determined in the control structure approximately corresponds to the output voltage of the inverter. In the case of speed measurements, it turns out that any phase shifts introduced by filters disrupt the operation of the estimator, and the best solution is to approximate the position derivative using numerical methods.

Based on the experimental research conducted, it can be concluded that the VCS model is the least accurate and that the constant resistance and inductance parameters do not reflect the actual operating conditions of the drive. During the optimisation of the estimator model parameters using the PSO algorithm, the obtained values minimised the objective function, i.e., the error between the estimated and measured current values, across the entire operating range of the drive thus averaging those values. The second proposed model, LUTE, which takes into account non-linear changes in flux as a function of currents, shows a significantly better correlation between measured and estimated currents, as demonstrated by Pearson's correlation coefficient (r = 0.99308 for VCS and r = 0.99862 for

LUTE). However, this model reflects only the average flux value for a fixed operating point. The most accurate model is ELUTE, which takes into account the dependence of the flux on the rotor position, thus allowing the estimated currents to reflect the local dynamic changes in the measured currents much more accurately. However, the improvement in the RMSE value of the ELUTE estimation error relative to LUTE is small.

The clear advantage of ELUTE over other estimators is evident from the studies on the impact of estimators in the SCL on THD of measured currents. It shows that, of the three estimators presented, ELUTE has the least impact on the THD content of measured currents. However, it is difficult to determine the impact of estimators on THD when the drive speed approaches the rated speed. Under such conditions, THD is reduced compared to a system operating without estimators. A thorough explanation of this phenomenon requires further research.

An important aspect of this work is the hardware implementation, which is comparable for each estimator. This is possible through the use of LUT tables with parameters determined offline, which are quick to access, and whose only disadvantage is increased memory requirements. While in the case of the LUTE estimator, the LUT size is not particularly large (several hundred values depending on the size of the measurement grid), in the case of ELUTE, it increases several hundred times depending on the resolution with which the dependence of the fluxes on the position angle is calculated.

Acknowledgements

This work was supported by the National Science Centre Poland under grant number 2021/41/B/ST7/02971.

References

Adamczyk, M. and Orlowska-Kowalska, T. (2022). Postfault Direct Field-Oriented Control of Induction Motor Drive Using Adaptive Virtual Current Sensor. *IEEE Transactions on Industrial Electronics*, 69, pp. 3418–3427. doi: 10.1109/TIE.2021.3075863

Armando, E., Bojoi, R. I., Guglielmi, P., Pellegrino, G. and Pastorelli, M. (2013). Experimental Identification of the Magnetic Model of Synchronous Machines. *IEEE Transactions on Industry Applications*, 49, pp. 2116–2125. doi: 10.1109/TIA.2013.2258876

Azzoug, Y., Sahraoui, M., Pusca, R., Ameid, T., Romary, R. and Cardoso, A. J. M. (2020). Current Sensors Fault Detection and Tolerant Control Strategy for Three-Phase Induction Motor Drives. *Electrical Engineering*, 103, pp. 881–898. doi: 10.1007/s00202-020-01120-5

Bedetti, N., Calligaro, S. and Petrella, R. (2015). Self-Commissioning of Inverter Dead-Time Compensation by Multiple Linear Regression Based on a Physical Model. *IEEE Transactions on Industry Applications*, 51, pp. 3954–3964. doi: 10.1109/TIA.2015.2436882

Bojoi, A., Pescetto, P., Ferrari, S. and Pellegrino, G. (2024). Experimental identification of the dqθ flux maps of synchronous machines. *2024 International Conference on Electrical Machines (ICEM)*, Torino, Italy, 2024, pp. 1–7, doi: 10.1109/ICEM60801.2024.10700160.

Das, S. and Manohar, M. (2023). A Resilient Current Sensor Fault-Tolerant Strategy for Vector-Controlled Induction Motor Drive. *IEEE Journal of Emerging and Selected Topics in Power Electronics*, 11, pp. 4313–4320. doi: 10.1109/JESTPE.2022.3179319

Dybkowski, M. and Jankowska, K. A. (2022). Universal System for Detection and Compensation of Current Sensor Faults in Three-Phase Power Electronic Systems. *Power Electronics and Drives*, 7, pp. 267–278. doi: 10.2478/pead-2022-0020

Hamming, R. W. (1989). *Digital Filters*, 3rd ed. Prentice Hall International (UK) Ltd., GBR.

Holtz, J. (2006). Sensorless Control of Induction Machines—With or Without Signal Injection? *IEEE Transactions on Industrial Electronics*, 53, pp. 7–30. doi: 10.1109/TIE.2005.862324

Liu, L., Liu, W. and Cartes, D. A. (2008). Particle Swarm Optimization-Based Parameter Identification Applied to Permanent Magnet Synchronous Motors. *Engineering Applications of Artificial Intelligence*, 21, pp. 1092–1100. doi: 10.1016/j.engappai.2007.10.002

Liu, Z. H., Wei, H. L., Li, X. H., Liu, K. and Zhong, Q. C. (2018). Global Identification of Electrical and Mechanical Parameters in PMSM Drive Based on Dynamic Self-Learning PSO. *IEEE Transactions on Power Electronics*, 33, pp. 10858–10871. doi: 10.1109/TPEL.2018.2801331

Manohar, M. and Das, S. (2017). Current Sensor Fault-Tolerant Control for Direct Torque Control of Induction Motor Drive Using Flux-Linkage Observer. *IEEE Transactions on Industrial Informatics*, 13, pp. 2824–2833. doi: 10.1109/TII.2017.2714675

Miniach, M. and Orlowska-Kowalska, T. (2025). Innovative Extended Kalman Filter in a Coherent System for Detection and Compensation of Various Current Sensor Faults in the Induction Motor Drive. *IEEE Transactions on Industrial Electronics*, vol. 72, no. 8, pp. 7772-7784, doi: 10.1109/TIE.2025.3528487.

Orlowska-Kowalska, T. (2003). *Sensorless Induction Motor Drives, Wroclaw University of Technology Press*. Wroclaw, Poland: Wroclaw University of Technology Press.

Romero-Laguna, A., Ibarra, L. and Galluzzi, R. (2024). Performance analysis of field oriented control under parametric variations of a PMSM. *2024 International Symposium on Electromobility (ISEM*), Guadalajara, Mexico, 2024, pp. 1-6, doi: 10.1109/ISEM62699.2024.10786768.

Savitzky, A. and Golay, M. J. E. (1964). Smoothing and Differentiation of Data by Simplified Least Squares Procedures. *Analytical Chemistry*, 36, pp. 1627–1639. doi: 10.1021/ac60214a047

Skowron, M., Jamshidpour, E., Teler, K., Orlowska-Kowalska, T. and Haghgooei, P. (2023). Current sensor fault detection and compensation system for wound rotor synchronous motor based on neural networks. *2023 IEEE Transportation Electrification Conference and Expo, Asia-Pacific (ITEC Asia-Pacific)*, Chiang Mai, Thailand, 2023, pp. 1-5, doi:10.1109/ITECAsia-Pacific59272.2023.10372315.

Teler, K., Skowron, M. and Orłowska-Kowalska, T. (2023). Implementation of MLP-Based Classifier of Current Sensor Faults in Vector-Controlled Induction Motor Drive. *IEEE Transactions on Industrial Informatics*, vol. 20, no. 4, pp. 5702-5713, doi: 10.1109/TII.2023.3336348.

Teler, K., Skowron, M. and Orlowska-Kowalska, T. (2025a). Analysis of the impact of stator phase current sensor faults on the performance of a permanent magnet motor drive. *2025 International Conference on Electrical Drives and Power Electronics (EDPE)*, Dubrovnik, Croatia, 2025, pp. 1-6, doi: 10.1109/EDPE66853.2025.11224199.

Teler, K., Skowron, M. and Orlowska-Kowalska, T. (2025b). Phase current estimation in PMSM drives using open-loop observers. *2025 International Conference on Electrical Drives and Power Electronics (EDPE)*, Dubrovnik, Croatia, 2025, pp. 1-6, doi: 10.1109/EDPE66853.2025.11224199.

Venghi, L. E., Aguilera, F., De La Barrera, P. M. and De Angelo, C. H. (2021). Current-sensors fault tolerant control system for electric drives: Experimental validation. *2021 XIX Workshop on Information Processing and Control (RPIC)*, SAN JUAN, Argentina, 2021, pp. 1-6, doi: 10.1109/RPIC53795.2021.9648522.

Xiahou, K. S., Lin, X. and Wu, Q. H. (2017). Current sensor fault-tolerant control of DFIGs using stator current regulators and Kalman filters. *2017 IEEE Power and Energy Society General Meeting*, Chicago, IL, USA, 2017, pp. 1-5, doi: 10.1109/PESGM.2017.8274498.

Zhu, Z. Q., Liang, D. and Liu, K. (2021). Online Parameter Estimation for Permanent Magnet Synchronous Machines: An Overview. *IEEE Access*, 9, pp. 59059–59084. doi: 10.1109/ACCESS.2021.3072959

Zuo, S., Huang, Z., Wu, Z. and Liu, C. (2023a). Improved Mathematical Model and Modeling of Permanent Magnet Synchronous Motors Considering Saturation, Spatial Harmonics, Iron Loss and Deadtime Effect. *Arabian Journal for Science and Engineering*, 48, pp. 6939–6955. doi: 10.1007/s13369-022-07507-9

Zuo, Y., Ge, X., Chang, Y., Chen, Y., Xie, D., Wang, H. and Woldegiorgis, A. T. (2023b). Current Sensor Fault-Tolerant Control for Speed-Sensorless Induction Motor Drives Based on the SEPLL Current Reconstruction Scheme. *IEEE Transactions on Industry Applications*, 59, pp. 845–856. doi: 10.1109/TIA.2022.3204733